Solar Energy 174 (2018) 593–605

Contents lists available at ScienceDirect

Solar Energy

journal homepage: www.elsevier.com/locate/solener

Effect of climate on electrical performance of finned phase change material integrated solar photovoltaic

Sourav Khanna[a,*], K.S. Reddy[b], Tapas K. Mallick[a,*]

[a] Environment and Sustainability Institute, Penryn Campus, University of Exeter, Cornwall TR10 9FE, United Kingdom
[b] Heat Transfer and Thermal Power Laboratory, Department of Mechanical Engineering, Indian Institute of Technology Madras, Chennai 600 036, India

ABSTRACT

Photovoltaic (PV) cells absorb the incident solar radiation while operation of which, majority part causes heating leading to the hampered electrical efficiency. PVs can be integrated with phase change material (PCM) to maintain cell temperature within desired limits and the effect can be improved by deploying fins. The current work aims at analysing the effect of climate on the electrical performance of finned PCM integrated PV. Modelling of system has been done which has been validated using experimental results. For the study, fins with various spacings, thicknesses and lengths are used. The main conclusions of the study are, (a) for less alterative climate, the improvement in the PV electrical output (using finned PCM) is 9.7%, 10.8%, 11.3%, 11.6% and 11.6% respectively for a spacing of 1 m, 1/2 m, 1/3 m, 1/4 m and 1/5 m. For highly alterative climate, the respective values reduce to 6.6%, 7.6%, 8.1%, 8.4% and 8.4%, (b) for warmer climate, the output increases by 10.1%, 11.3%, 11.8%, 12.1% and 12.1% while for colder climate, it increases only by 5.4%, 6.1%, 6.5%, 6.7% and 6.7%, (c) for windy climate, the power increments are significantly lesser as compared to the other case, (d) climate having higher wind azimuth results in better performance of finned PCM, and (e) for clear sky climate, performance of finned PCM is better.

1. Introduction

The temperature rise of photovoltaic (PV) adversely affects its electrical performance (Kaplani and Kaplanis, 2014; Khanna et al., 2017). In the current section, the experimental and theoretical studies for the passive cooling of PV using phase change material (PCM) have been presented.

1.1. Experimental studies

Baygi and Sadrameli (2018) have studied the thermal variations of PV using polyethylene glycol as PCM for the climate of Tehran, Iran. The results conclude that the PCM decreases the PV temperature from 60 °C to 45 °C. Huang et al. (2006, 2007) have investigated the thermal variations of an imitated PV system integrated with paraffin wax 25 PCM. The results conclude that the temperature rise of the PV can be reduced from 62 °C to 36 °C using PCM and from 62 °C to 26 °C using finned PCM. Hasan et al. (2015) have investigated the PV-PCM system for two different weather conditions (Dublin and Vehari). It is shown that for Dublin, the largest temperature drop in PV is from 49 °C to 39 °C and for Vehari, it is from 63 °C to 41.5 °C using $CaCl_2$ $6H_2O$ PCM. Indartono et al. (2014) have compared roof integrated PV and stand integrated PV systems for the climate of Indonesia using vaselinum flavum PCM. It is shown that a decrease in the PV temperature from 60 °C to 54.3 °C can be achieved for roof integrated system and from 44.8 °C to 42.2 °C for stand integrated system. Hasan et al. (2010) have analysed five different PCMs. It is shown that the largest PV temperature drop can be achieved from 57 °C to 39 °C using $CaCl_2$ and C-P. Kamkari and Groulx (2018) have investigated the melting rate of PCM by applying heat source at bottom using lauric acid as PCM and found that the horizontal position of the system leads to faster melting than that of vertical position. Sharma et al. (2016) have used paraffin wax 42 PCM integrated with asymmetric compound parabolic CPV. The PV temperature drop from 60 °C to 51 °C is shown. Sharma et al. (2017) have used a nano enhanced PCM with micro finned arrangement for cooling and shown a drop of 12.5 °C in the PV temperature. Preet et al. (2017) have analysed the PV and PVT-PCM systems at Gurdaspur using paraffin wax 30 PCM and reported a decrease of PV temperature from 80 °C to 55 °C. Browne et al. (2016a, 2016b) and Browne et al. (2015) have used eutectic mixture of capric and palmitic fatty acids as PCM. An enhancement of 5.5 °C in the water temperature is achieved using PVT-PCM as compared to PVT system. Su et al. (2018) have studied the tracking integrated CPV-T and CPV-T-PCM systems. An enhancement of 10% in the electrical efficiency is achieved using paraffin wax PCM at Macau. Many theoretical studies are also carried out by researchers (Browne et al., 2015; Ma et al., 2015; Du et al., 2013; Shukla et al., 2017; Chandel and Agarwal, 2017; Preet, 2018).

* Corresponding authors.
E-mail addresses: s.khanna@exeter.ac.uk (S. Khanna), t.k.mallick@exeter.ac.uk (T.K. Mallick).

https://doi.org/10.1016/j.solener.2018.09.023
Received 8 May 2018; Received in revised form 7 September 2018; Accepted 11 September 2018
Available online 24 September 2018

Nomenclature

A_{PV}	aperture area of PV panel (m^2)
C_p	specific heat (J/kg K)
D	heat of fusion's distribution function during change of phase
E	electrical output (W)
F	shape factor
g	acceleration due to gravity (m/s^2)
Gr	Grashof number
h	convective heat transfer coefficient (W/m^2 K)
H_f	heat of fusion (J/kg)
I_T	incident solar flux on PV (W/m^2)
k	thermal conductivity (W/m K)
l	part of total PCM mass in liquefied form
L	length of system (m)
L_{ch}	characteristic length (m)
L_f	length of fins (m)
Nu	Nusselt number
p	pressure (Pa)
Pr	Prandtl number
Ra	Rayleigh number
s_f	distance between fins (m)
t	time (s); thickness (m)
T	temperature (K)
t_f	fin's thickness (m)
T_m	phase change material's melting temperature (K)
$T_{P,s}$	temperature below which whole PCM is fully solid (K)
$T_{P,l}$	temperature above which PCM is fully liquid (K)
t_{si}	silicon thickness (m)
u	phase change material's velocity (m/s)
v_w	wind velocity (m/s)

Greek symbols

β	inclination angle of the system (rad)
β_c	temperature coefficient (/K)
γ_w	wind azimuth angle (rad)
γ_c	solar irradiance coefficient
δ	box's depth (m)
ε	emissivity for reradiation
η	electrical efficiency of PV
μ	dynamic viscosity of phase change material (kg/ms)
ρ	density of the material (kg/m^3)
σ	Stefan–Boltzmann constant ($W/m^2 K^4$)
$(\tau\alpha)_{eff}$	effective product of transmissivity of glass cover and absorptivity of solar cell
υ	kinematic viscosity of air (m^2/s)

Abbreviations

EVA	ethylene vinyl acetate
PCM	phase change material
PV	photovoltaic
STC	standard test conditions

Subscripts

a	ambient
al	aluminium
avg	average
c	critical
f	forced
gl	glass
gr	ground
l	liquid phase
P	PCM
s	solid phase
si	silicon
sk	sky
STC	standard test conditions
te	tedlar
x	along length
y	along depth

1.2. Theoretical studies

Brano et al. (2014) and Ciulla et al. (2012) have used forward difference model for time and first-order central difference model for the space derivative. The experimental and the computed results match significantly with maximum deviations being −6.53 °C to +7.55 °C using paraffin wax 27 as PCM at Italy. Atkin and Farid (2015) have studied the infusion of PCM into graphite for the thermal regulation. The results show an enhancement of 7% in the electrical efficiency. Kibria et al. (2016) have used fully implicit model for enthalpy formulation of PCM. For simulation, paraffin wax 20, 25 and 28 are used for the climate of Dhahran. The results conclude that after eight hours of charging, first PCM becomes liquid completely. However, for second and third PCM, only 0.8 and 0.65 portions become liquid. Biwole et al. (2013, 2018) and Groulx and Biwole (2014) have modelled the drastic shift PCM undergoes during phase change and shown that the same must be modelled and handled with care as the chances for divergence and errors are immense. Mahamudul et al. (2016) have used paraffin wax 35 and reported a drop in PV temperature from 51 °C to 41 °C at university of Malaya. Kant et al. (2016) have reported that the consideration of conduction in PCM leads to drop in PV temperature from 60 °C to 58.5 °C and the consideration of both conduction and convection in PCM leads to drop in the PV temperature from 60 °C to 55 °C using paraffin wax 35 for the climate of Uttar Pradesh. Park et al. (2014) have worked on finding the optimal melting temperature of PCM for the climatic conditions of Incheon and 25 °C is reported as the optimum one. The effect of installation direction on the optimum PCM quantity is also investigated. Su et al. (2017b) have optimized the melting temperature of PCM for maximum energy output from PVT-PCM system at Ninjangh and reported that the PCM with melting temperature of 40 °C is the best. Khanna et al. (2018a, 2017, 2018b, 2018c, 2018d, 2018f) and Al Siyabi et al. (2018a, 2018b) have worked on analysing the effect of operating conditions and optimization of PCM quantity for different working conditions, daily solar irradiance levels and system dimensions. Emam and Ahmed (2017) have analysed different configurations of PCM heat sinks and concluded that the parallel cavities are better than the series ones. Huang et al. (2004, 2011) have investigated the thermal variations of an imitated PV system integrated with finned PCM. It has been found that the temperature rise of the PV can be reduced from 87 °C to 38 °C using paraffin wax 32 as PCM and from 87 °C to 35 °C using finned PCM. Emam et al. (2017) have studied the influence of tilt angle of the concentrated PV-PCM. It is shown that the slanted system is better compared to vertical or horizontal. Cui et al. (2016) have integrated the CPV thermoelectric system with PCM and found a 25% drop in the PV temperature using NaOH-KOH PCM at Nanjing. Su et al. (2017a) have integrated air based PVT system with paraffin. It is shown that the use of PCM drops the PV temperature from 77 °C to 69 °C for the climate of Nanjing. The method of separation of variables is also applied by researchers to derive explicit analytical expressions for temperature distribution (Khanna et al., 2016) incorporating the effect of non-uniform solar flux distribution (Khanna and Sharma, 2016; Sharma et al., 2016), thermal variations (Khanna

and Sharma, 2015, 2016) and angle of incidence of sun rays (Khanna et al., 2014) which can be helpful in computing temperature distribution in PV-PCM system.

Thus, performance study of PCM integrated PVs has been reported in literature. However, climatic conditions for which a particular finned PCM would work best/worst are not laid down. In the previous work, the current authors have analysed the PV-PCM system (Khanna et al., 2018e). Thus, the current work aims at analysing the effect of climate on Finned-PV-PCM's electrical performance.

2. Methodology

Current investigation involves two setups: one being PV-alone and the other being finned-PCM integrated PV as depicted in Fig. 1. PCM box has the fins attached within. The whole assembly of PV and PCM box is kept at an inclination of β. PV panel is a typical stack of five films. The PCM box is L meter long and δ meter deep. Fins' dimensions viz. length, spacing and width have been denoted by L_f, s_f, and w_f.

The assumptions made in the investigation are as follows

(i) The PV surface is exposed to a uniform solar radiation spread
(ii) Insulation applied on side-walls and rear leads to adiabatic condition at respective walls
(iii) PV layers and PCM individual phases are isotropic and homogeneously distributed.
(iv) PV's traits do not change with temperature (thermal dependency of efficiency is, however, accounted for).
(v) PCM's thermal traits in individual phases do not change with temperature.
(vi) Thermal resistance by layers' interfaces is neglected.

Analytical modelling for system's components has been done subsequently.

2.1. Glass

At any instant t, the temperature profiles along the length and depth of the topmost glass can be found solving the following equation

$$\rho_{gl} C_{p,gl} \frac{\partial T_{gl}}{\partial t} = k_{gl}\left(\frac{\partial^2 T_{gl}}{\partial x^2} + \frac{\partial^2 T_{gl}}{\partial y^2}\right) \tag{1}$$

subjected to the following boundary and initial conditions

$$k_{gl}\frac{\partial T_{gl}}{\partial y} = h_c[T_{gl}-T_a] + F_{gl\_sk}\sigma\varepsilon_{gl}[T_{gl}^4-T_{sk}^4] + F_{gl\_gr}\sigma\varepsilon_{gl}[T_{gl}^4-T_{gr}^4] \quad at\ \ glass\ \ top \tag{2}$$

$$k_{gl}\frac{\partial T_{gl}}{\partial x} = 0 \quad at\ \ edges\ \ of\ \ glass \tag{3}$$

$$k_{gl}\frac{\partial T_{gl}}{\partial y} = k_{EVA}\frac{\partial T_{EVA1}}{\partial y} \quad at\ \ glass{-}EVA\ \ interface \tag{4}$$

$$T_{gl} = T_a \quad when\ \ t = 0 \tag{5}$$

where the symbols have their respective meanings as per the nomenclature. Eq. (2) shows the convective heat transfer from glass to ambient, radiative heat transfer from glass to sky and from glass to ground. h_c is calculated incorporating both the forced and natural effects of convection. The natural effect is calculated in terms of Nusselt number as follows (Khanna et al., 2017)

$$Nu = \begin{cases} [0.13(Gr\ \ Pr)^{1/3}] & if\ \ \beta \le 30° \\ [0.13\{(Gr\ \ Pr)^{1/3}-(Gr_c\ \ Pr)^{1/3}\} + 0.56(Gr_c\ \ Pr\sin\beta)^{1/4}] & if\ \ \beta > 30° \end{cases} \tag{6}$$

where Pr is the Prandtl number of air calculated from its thermal properties at a temperature of $0.75T_{gl,avg} + 0.25T_a$ (Kaplani and Kaplanis, 2014). Gr is the Grashof number defined as follows (Kaplani and Kaplanis, 2014)

$$Gr = \frac{g(T_{gl,avg}-T_a)L_{ch}^3}{(0.25T_{gl,avg} + 0.75T_a)\upsilon^2} \tag{7}$$

The forced effect of convection incorporating the effect of wind speed and wind azimuth is calculated as (Khanna et al., 2017)

$$h_f = 0.848k_a[\sin\beta\cos\gamma_w v_w \mathrm{Pr}/\upsilon]^{1/2}(L_{ch}/2)^{-1/2} \tag{8}$$

where L_{ch} is the characteristic length defined as the length of surface along the direction of flow. In Eq. (2), the radiative heat transfer involves the view factors from glass to sky ($F_{gl\_sk} = 0.5 + 0.5\cos\beta$) and glass to ground ($F_{gl\_sk} = 0.5–0.5\cos\beta$) (Kaplani and Kaplanis, 2014).

2.2. First EVA layer

At any instant t, the temperature profiles along the length and depth of the first EVA layer can be found solving the following equation

$$\rho_{EVA} C_{p,EVA} \frac{\partial T_{EVA1}}{\partial t} = k_{EVA}\left(\frac{\partial^2 T_{EVA1}}{\partial x^2} + \frac{\partial^2 T_{EVA1}}{\partial y^2}\right) \tag{9}$$

subjected to the following boundary and initial conditions

$$k_{EVA}\frac{\partial T_{EVA1}}{\partial x} = 0 \quad at\ \ edges\ \ of\ \ EVA \tag{10}$$

$$k_{EVA}\frac{\partial T_{EVA1}}{\partial y} = k_{si}\frac{\partial T_{si}}{\partial y} \quad at\ \ EVA{-}silicon\ \ interface \tag{11}$$

$$T_{EVA1} = T_a \quad when\ \ t = 0 \tag{12}$$

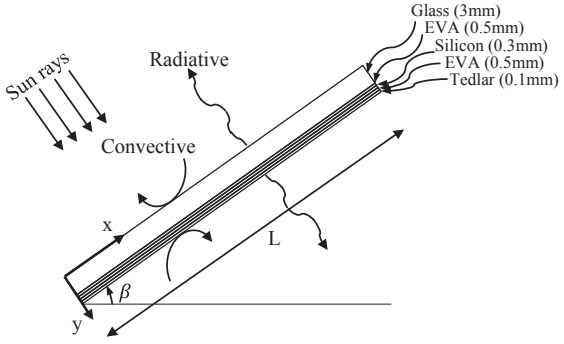

(a) PV-alone setup

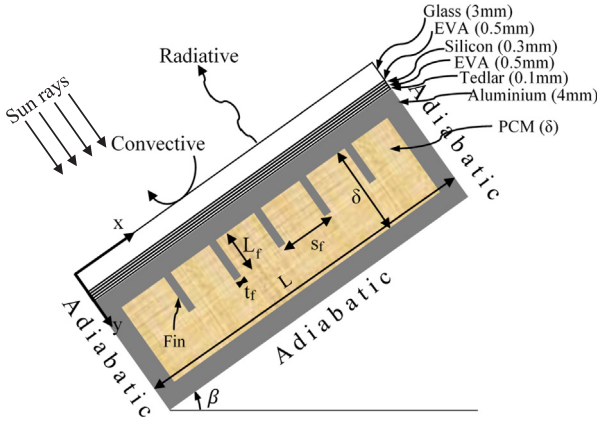

(b) finned-PV-PCM setup

Fig. 1. Setups studied under current investigation (Khanna et al., 2018b).

2.3. Silicon

At any instant *t*, the temperature profiles along the length and depth of the silicon layer can be found solving the following equation

$$\rho_{si}C_{p,si}\frac{\partial T_{si}}{\partial t} = k_{si}\left(\frac{\partial^2 T_{si}}{\partial x^2} + \frac{\partial^2 T_{si}}{\partial y^2}\right) + \left[(\tau\alpha)_{eff}I_T - \eta_{STC}I_T\left\{1 + \beta_c(T_{PV}-25) + \gamma_c \ln\left(\frac{I_T}{1000}\right)\right\}\right]/t_{si} \quad (13)$$

subjected to the following boundary and initial conditions

$$k_{si}\frac{\partial T_{si}}{\partial x} = 0 \quad at\ \ edges\ \ of\ \ silicon \quad (14)$$

$$k_{si}\frac{\partial T_{si}}{\partial y} = k_{EVA}\frac{\partial T_{EVA2}}{\partial y} \quad at\ \ silicon{-}EVA\ \ interface \quad (15)$$

$$T_{si} = T_a \quad when\ \ t = 0 \quad (16)$$

2.4. Second EVA layer

At any instant t, the temperature profiles along the length and depth of the second EVA layer can be found solving the following equation

$$\rho_{EVA}C_{p,EVA}\frac{\partial T_{EVA2}}{\partial t} = k_{EVA}\left(\frac{\partial^2 T_{EVA2}}{\partial x^2} + \frac{\partial^2 T_{EVA2}}{\partial y^2}\right) \quad (17)$$

subjected to the following boundary and initial conditions

$$k_{EVA}\frac{\partial T_{EVA2}}{\partial x} = 0 \quad at\ \ edges\ \ of\ \ EVA \quad (18)$$

$$k_{EVA}\frac{\partial T_{EVA2}}{\partial y} = k_{te}\frac{\partial T_{te}}{\partial y} \quad at\ \ EVA{-}tedlar\ \ interface \quad (19)$$

$$T_{EVA2} = T_a \quad when\ \ t = 0 \quad (20)$$

2.5. Tedler

At any instant t, the temperature profiles along the length and depth of the tedlar can be found solving the following equation

$$\rho_{te}C_{p,te}\frac{\partial T_{te}}{\partial t} = k_{te}\left(\frac{\partial^2 T_{te}}{\partial x^2} + \frac{\partial^2 T_{te}}{\partial y^2}\right) \quad (21)$$

subjected to the following boundary and initial conditions

$$k_{te}\frac{\partial T_{te}}{\partial x} = 0 \quad at\ \ edges\ \ of\ \ tedlar \quad (22)$$

$$k_{te}\frac{\partial T_{te}}{\partial y} = \begin{cases} h_c[T_{te}-T_a] + F_{te\_sk}\sigma\varepsilon_{te}[T_{te}^4-T_{sk}^4] + F_{te\_gr}\sigma\varepsilon_{te}[T_{te}^4-T_{gr}^4] \\ \qquad at\ \ rear\ \ PV\ \ alone \\ k_{al}\frac{\partial T_{al}}{\partial y} \quad at\ \ tedlar{-}aluminium\ \ interface \end{cases} \quad (23)$$

$$T_{te} = T_a \quad when\ \ t = 0 \quad (24)$$

For PV-alone system, Eq. (23) shows the convective heat transfer from tedlar to ambient, radiative heat transfer from tedlar to sky and from tedlar to ground. h_c is calculated incorporating both the forced and natural effects of convection. The natural effect is calculated in terms of Nusselt number as follows (Khanna et al., 2017)

$$Nu = \begin{cases} 0.58(Ra)^{1/5} & if\ \ \beta \le 2° \\ 0.56(Ra\sin\beta)^{1/5} & if\ \ 2° < \beta < 30° \\ \left[0.825 + \frac{0.387(Ra\sin\beta)^{1/6}}{\{1+(0.492/Pr)^{9/16}\}^{8/27}}\right]^2 & if\ \ \beta \ge 30° \end{cases} \quad (25)$$

The forced effect of convection incorporating the effect of wind speed and wind azimuth is calculated as (Khanna et al., 2017)

$$h_f = \begin{cases} 3.83v_w^{0.5}L_{ch}^{-0.5} & for\ \ laminar\ \ flow \\ 5.74v_w^{0.8}L_{ch}^{-0.2} - 16.46L_{ch}^{-1} & for\ \ mixed\ \ flow \\ 5.74v_w^{0.8}L_{ch}^{-0.2} & for\ \ fully\ \ turbulent\ \ flow \end{cases} \quad (26)$$

where L_{ch} is the length towards the wind direction.

2.6. Aluminium box with fins

At any instant *t*, the temperature profiles along the length and depth of the aluminium container with fins can be found solving the following equation

$$\rho_{al}C_{p,al}\frac{\partial T_{al}}{\partial t} = k_{al}\left(\frac{\partial^2 T_{al}}{\partial x^2} + \frac{\partial^2 T_{al}}{\partial y^2}\right) \quad (27)$$

subjected to the following boundary and initial conditions

$$k_{al}\frac{\partial T_{al}}{\partial x} = 0 \quad at\ \ edges\ \ of\ \ aluminium\ \ box \quad (28)$$

$$k_{al}\frac{\partial T_{al}}{\partial y} = k_P\frac{\partial T_P}{\partial y} \quad at\ \ aluminium{-}PCM\ \ interface\ \ along\ \ box\ \ length \quad (29)$$

$$k_{al}\frac{\partial T_{al}}{\partial x} = k_P\frac{\partial T_P}{\partial x} \quad at\ \ aluminium{-}PCM\ \ interface\ \ along\ \ box\ \ depth \quad (30)$$

$$k_{al}\frac{\partial T_{al}}{\partial y} = 0 \quad at\ \ rear\ \ of\ \ aluminium\ \ box \quad (31)$$

$$T_{al} = T_a \quad when\ \ t = 0 \quad (32)$$

2.7. PCM

At any instant *t*, the temperature profiles along the length and depth of the PCM can be found solving the following equations

$$\rho_P C_{p,P}\frac{\partial T_P}{\partial t} = \nabla\cdot(k_P\nabla T_P) - \frac{\partial}{\partial x}(\rho_P C_{p,P}u_x T_P) - \frac{\partial}{\partial y}(\rho_P C_{p,P}u_y T_P) \quad (33)$$

$$\rho_P\frac{\partial \vec{u}}{\partial t} + \rho_P(\vec{u}\cdot\nabla)\vec{u} = -\frac{\partial p}{\partial x} + \mu_P\nabla^2\vec{u} + \rho_P\vec{g} \quad (34)$$

$$\nabla\cdot\vec{u} = 0 \quad (35)$$

subjected to the following boundary and initial conditions

$$k_P\frac{\partial T_P}{\partial y} = k_{al}\frac{\partial T_{al}}{\partial y} \quad for\ \ aluminium{-}PCM\ \ interface\ \ along\ \ box\ \ length \quad (36)$$

$$k_P\frac{\partial T_P}{\partial x} = k_{al}\frac{\partial T_{al}}{\partial x} \quad for\ \ aluminium{-}PCM\ \ interface\ \ along\ \ box\ \ depth \quad (37)$$

$$T_P = T_a \quad when\ \ t = 0 \quad (38)$$

$$u_x = u_y = 0 \quad for\ \ every\ \ inside\ \ surface\ \ of\ \ PCM\ \ box \quad (39)$$

$$u_x = u_y = 0 \quad when\ \ t = 0 \quad (40)$$

Next challenge is to model the drastic shift PCM undergoes during phase change vis a vis its thermal traits. The same must be modelled and handled with care as the chances for divergence and errors are immense. Thus, $l(T)$, the part of total PCM mass in liquefied form, satisfies the following 2nd order differentiable function (making sure the convergence is achieved) (Biwole et al., 2013).

$$l(T) = \sum_{i=0}^{6} a_i T^i \quad (41)$$

subjected to the following boundary conditions

$$l_{at\ \ T_{P,s}} = 0, \quad l_{at\ \ T_m} = \frac{1}{2}, \quad l_{atT_{P,l}} = 1 \tag{42}$$

$$\frac{dl}{dT}_{at\ \ T_{P,s}} = \frac{d^2l}{dT^2}_{at\ \ T_{P,s}} = \frac{dl}{dT}_{at\ \ T_{P,l}} = \frac{d^2l}{dT^2}_{at\ \ T_{P,l}} = 0 \tag{43}$$

The relations given by Eqs. (42) and (43) lead to solution of (Eq. (41)) and estimation of the coefficients a_0, a_1, a_2, a_3, a_4, a_5 and a_6 in following manner

$$\begin{bmatrix} a_0 \\ a_1 \\ a_2 \\ a_3 \\ a_4 \\ a_5 \\ a_6 \end{bmatrix} = \begin{bmatrix} 1 & T_{P,s} & T_{P,s}^2 & T_{P,s}^3 & T_{P,s}^4 & T_{P,s}^5 & T_{P,s}^6 \\ 1 & T_m & T_m^2 & T_m^3 & T_m^4 & T_m^5 & T_m^6 \\ 1 & T_{P,l} & T_{P,l}^2 & T_{P,l}^3 & T_{P,l}^4 & T_{P,l}^5 & T_{P,l}^6 \\ 0 & 1 & 2T_{P,s} & 3T_{P,s}^2 & 4T_{P,s}^3 & 5T_{P,s}^4 & 6T_{P,s}^5 \\ 0 & 0 & 2 & 6T_{P,s} & 12T_{P,s}^2 & 20T_{P,s}^3 & 30T_{P,s}^4 \\ 0 & 1 & 2T_{P,l} & 3T_{P,l}^2 & 4T_{P,l}^3 & 5T_{P,l}^4 & 6T_{P,l}^5 \\ 0 & 0 & 2 & 6T_{P,l} & 12T_{P,l}^2 & 20T_{P,l}^3 & 30T_{P,l}^4 \end{bmatrix}^{-1} \begin{bmatrix} 0 \\ 1/2 \\ 1 \\ 0 \\ 0 \\ 0 \\ 0 \end{bmatrix} \tag{44}$$

In order to model the solid and liquid portions of the PCM, its cooler portion having $T < T_{P,s}$ is assumed to be a highly viscous fluid which can be equated to the state of the solid phase. Similarly, the hotter portion having $T > T_{P,l}$ is modelled as a very less viscous fluid. In this way, the viscosity satisfies the following expression (Biwole et al., 2013)

$$\mu(T) = \mu_l \left[1 + \frac{10^5\{1-l(T)\}^2}{l(T)^3 + 10^{-3}} \right] \tag{45}$$

The other thermal properties of phase change material as function of liquefied mass are modelled as

$$C_{p,P}(T) = \begin{cases} C_{p,P,s} & if \quad T < T_{P,s} \\ C_{p,P,s} + (C_{p,P,l} - C_{p,P,s})l(T) + H_f D(T) & if \quad T_{P,s} \le T \le T_{P,l} \\ C_{p,P,l} & if \quad T > T_{P,l} \end{cases} \tag{46}$$

$$\rho_P(T) = \begin{cases} \rho_{P,s} & if \quad T < T_{P,s} \\ \rho_{P,s} + (\rho_{P,l} - \rho_{P,s})l(T) & if \quad T_{P,s} \le T \le T_{P,l} \\ \rho_{P,l} & if \quad T > T_{P,l} \end{cases} \tag{47}$$

$$k_P(T) = \begin{cases} k_{P,s} & if \quad T < T_{P,s} \\ k_{P,s} + (k_{P,l} - k_{P,s})l(T) & if \quad T_{P,s} \le T \le T_{P,l} \\ k_{P,l} & if \quad T > T_{P,l} \end{cases} \tag{48}$$

2.8. Electrical output

The effects of average temperature of PV ($T_{PV,avg}$), solar irradiance at tilted PV (I_T), temperature coefficient (β_c), solar irradiance coefficient (γ_c), efficiency of PV panel at standard test conditions (η_{STC}) and area of PV (A_{PV}) on the electrical output of the systems are incorporated as follows (Kaplani and Kaplanis, 2014)

$$E = \eta_{STC} \left\{ 1 + \beta_c (T_{PV,avg} - 25) + \gamma_c \ln\left(\frac{I_T}{1000} \right) \right\} I_T A_{PV} \tag{49}$$

3. Solving approach

Both setups under investigation viz. PV-alone and Finned-PV-PCM have been constructed geometrically using two-dimensional model in ANSYS 17.1. Individual setup components: 5 PV layers, PCM, fins and box are constructed using 'Design Modeler'. In order to construct the interfaces, the contact surfaces of individual components are connected with each other using energy balance. The respective interfaces are joined using 'Wall coupling' to integrate the whole Finned-PV-PCM. System's walls are incorporated with the suitable boundary constraints. Meshing has been done using 'Face Meshing' with quadrilateral geometry (Fig. 2). 'Edge Sizing' has been used to generate the mesh by setting the number of divisions. It has been observed that results change by significant ± 1.5 °C if the number of elements in the mesh is increased to 50,000 from the initial 25,000. However, further increment in the number of elements to 100,000 doesn't lead to any significant improvement in results (± 0.2 °C). Similar study has been performed to fix the desired time interval as 0.1 s for which all the parameters are assumed to remain constant.

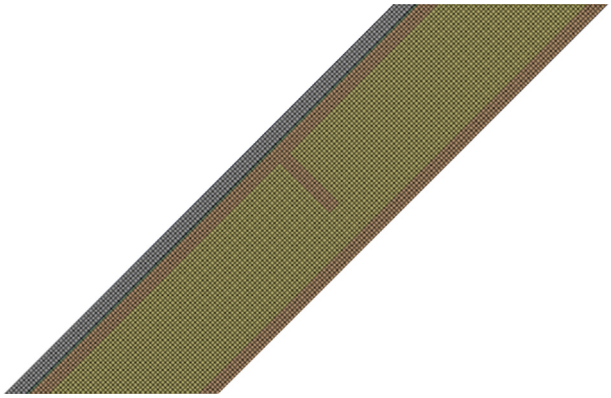

Fig. 2. Meshing of a portion of the system.

'Pressure-Based' type of solver has been applied for solving the equations. 'Planar' and 'Transient' modes have been applied for '2D Space' and 'Time' respectively. 'PRESTO', 'First Order Upwind' and 'First Order Upwind' discretization methods have been applied for 'Pressure', 'Energy' and 'Momentum' respectively.

4. Experimental validation

For the purpose of validating the proposed work experimentally, the work of Hasan et al. (2015) has been used. PCM used for the purpose was Calcium chloride hexahydrate. Polycrystalline PV panel having dimensions 771 mm × 665 mm integrated with 5 mm thick aluminium container (for PCM) having internal dimensions of 700 mm × 600 mm × 40 mm was used. Fins inside the container were deployed with a spacing of 75 mm. The system performance was studied under the ambient conditions of Vehari on 30th October. The current model has been applied with the same system. PV temperature's plot as function of time using proposed work is given in Fig. 3 and has been compared against the reported experimental work.

5. Results and discussion

Current investigation involves the computation of power produced and its dependency on time and different climates (in the month of June) for two setups under consideration: PV-alone and finned phase change material integrated PV considering polycrystalline silicon based PV panels. For the study, fins with different geometries have been studied. The improvement in power production with effective cooling in case of Finned-PV-PCM is reported too. Details of various thermal and geometrical properties of the two systems under investigation are tabulated in Table 1. The three PCMs chosen for the work have been RT – 18, 25 and 35 HC (Rubitherm Phase Change Material, 2018) respectively suitable for the typical outside temperatures in the respective

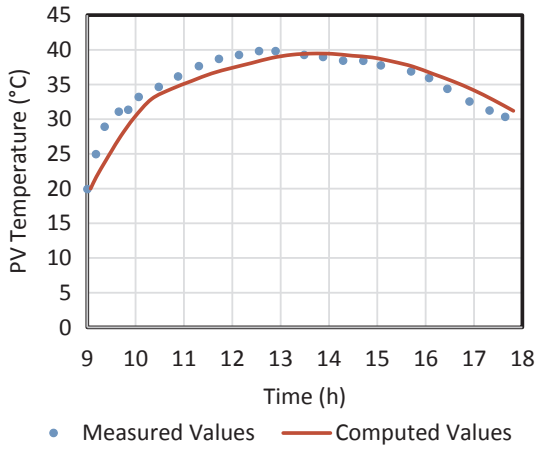

Fig. 3. Validation of proposed work with the reported experiments (Hasan et al., 2015).

Table 1
Thermophysical properties of system and paraffin wax 25 PCM.

Parameter	Value	Parameter	Value
A_{PV} (m^2)	1	t_{te} (mm)	0.1
$C_{p,al}$ (J/kg K)	903	L (m)	1
$C_{p,EVA}$ (J/kg K)	2090	$T_{P,s}$ (°C)	25.6
$C_{p,gl}$ (J/kg K)	500	$T_{P,l}$ (°C)	27.6
$C_{p,P,l}$ (J/kg K)	2400	β (°)	Latitude
$C_{p,P,s}$ (J/kg K)	1800	β_c (K^{-1})	−0.005
$C_{p,si}$ (J/kg K)	677	γ_c	0.085
$C_{p,te}$ (J/kg K)	1250	δ (cm)	6
H_f (J/kg)	232,000	ε_{gl}	0.85
k_{al} (W/m K)	211	ε_{te}	0.91
k_{EVA} (W/m K)	0.35	η_{STC}	0.20
k_{gl} (W/m K)	1.8	μ_l (kg/m-s)	0.001798
$k_{P,l}$ (W/m K)	0.18	ρ_{al} (kg/m^3)	2675
$k_{P,s}$ (W/m K)	0.19	ρ_{EVA} (kg/m^3)	960
k_{si} (W/m K)	148	ρ_{gl} (kg/m^3)	3000
k_{te} (W/m K)	0.2	$\rho_{P,l}$ (kg/m^3)	749
t_{al} (mm)	4	$\rho_{P,s}$ (kg/m^3)	785
t_{EVA} (mm)	0.5	ρ_{si} (kg/m^3)	2330
t_{gl} (mm)	3	ρ_{te} (kg/m^3)	1200
t_{si} (mm)	0.3	$(\tau\alpha)_{eff}$	0.9

climates. The PCMs are chosen such that all the thermophysical properties are almost same except the melting points. For the chosen cold climate, the ambient temperature remains lesser than 17 °C. Thus, RT18HC is used for cold climate. Similarly, RT35HC is used for hot climate. For hot climate, RT18 HC cannot be used for PV cooling due to the fact that it will remain melted during whole operation.

Five types of fins spacings have been chosen: s_f = 1 m, 1/2 m, 1/3 m, 1/4 m and 1/5 m. Since, length of the system is 1 m, s_f = 1 m corresponds to the case of no-fin. The case of s_f = 1/2 m corresponds to the fin position at the middle of the container. The case of s_f = 1/3 m corresponds to the fins at positions of 0.333 m and 0.666 m in the container. Similarly, the case of s_f = 1/4 m corresponds to the fins at positions of 0.25 m, 0.50 m and 0.75 m in the container.

5.1. Highly alterative vs lesser alterative climates

For different fin geometries, the electrical outputs from the two systems are found out for Madrid (40.4°N 3.7°W) and Benidorm (38.5°N 0.1°W) representing highly alterative and lesser alterative climates respectively and have been presented in Fig. 4. The climates of Madrid and Benidorm are chosen for the comparison due to the fact that they have almost similar solar irradiance profiles, similar average ambient temperature over the day, similar wind speeds (~3.5–4.0 m/s) and similar wind azimuth angles (~90°) but differ drastically in the variation in the ambient temperature over the day. Thus, the effect of highly alterative and lesser alterative features can be studied in isolation by studying these climates.

For highly alterative climate, the ambient temperature varies over the day within 17.9 °C to 30.1 °C and for lesser alterative climate, it varies within 22.7 °C to 24.8 °C (Fig. 4a). For former case, the PV electrical output increases from 164.9 W (in PV-alone) to 181.2 W, 183.1 W, 184.0 W, 184.5 W and 184.5 W (in Finned-PV-PCM) for s_f = 1 m, 1/2 m, 1/3 m, 1/4 m and 1/5 m respectively and for latter case, it increases from 166.1 W (in PV-alone) to 188.8 W, 190.7 W, 191.6 W, 192.1 and 192.1 (in Finned-PV-PCM) for respective s_f values (Fig. 4c).

The results show that for highly alterative climate, the increments in electrical output using finned phase change material are 6.6%, 7.6%, 8.1%, 8.4% and 8.4% for s_f = 1 m, 1/2 m, 1/3 m, 1/4 m and 1/5 m respectively (Fig. 4d), 7.3%, 7.6% and 8.4% for L_f = δ/3, 2δ/3 and δ respectively (Fig. 4e) and 7.4%, 8.0%, 8.4% and 8.4% for t_f = 0.5 mm, 1 mm, 2 mm and 4 mm respectively (Fig. 4f). For less alterative climate, the enhancements in electrical output increase to 9.7%, 10.8%, 11.3%, 11.6% and 11.6% for different spacings (Fig. 4d), 10.4%, 10.7% and 11.6% for different lengths (Fig. 4e) and 10.6%, 11.2%, 11.6% and 11.6% respectively for different thicknesses (Fig. 4f).

From numbers, it can be noted that finned phase change material is lesser useful if the outside temperature variation per day or month is more. Because, in that case, with higher temperatures outside, there would be significant amount of time in a day and month for which the PCM will always be in liquid state thereby having no operational use. Even if someone tries to use PCM having melting range on higher side of the temperature scale, still there would be a significant time for which it can't be used as it will remain solid until it reaches the higher temperature of fusion.

It must be mentioned that fin length, spacing and thickness are important parameters affecting the power generation from PV. The case of fin's length equalling depth of PCM box (δ) is the one having maximum power as compared to other lengths (Fig. 4f). When fin's length is δ, its tip comes in contact with the box's bottom and given the highly conducting characteristics of aluminium, the box's bottom absorbs heat and makes more PCM to melt nearby which was previously done only near fins and front. Thus, in this case, PCM extracts more heat from the system and thus cools the PV more effectively. Additionally, it can be observed that decrease in spacing beyond 25 cm (Fig. 4e) and increase in thickness beyond 2 mm (Fig. 4g) have marginal impact on electrical output. Thus, the most suitable fin geometry for power has been found as 25 cm of fins' spacing, length as box's depth and thickness as 2 mm.

5.2. Colder vs warmer climates

For different fin geometries, the electrical outputs from the two systems are found out for Monaco (43.7°N 7.4°E) and Chennai (13.1°N 80.3°E) representing colder and warmer climates respectively and have been presented in Fig. 5 respectively. The climates of Chennai and Monaco are chosen for the comparison due to the fact that they have almost similar solar irradiance profiles, similar alterative feature, similar wind speeds (~4.0–5.0 m/s) and similar wind azimuth angles (~0°) but differ drastically in the average ambient temperature. Thus, the effect of warmer and colder features can be studied in isolation by studying these climates.

For colder climate, the average ambient temperature over the day is around 16.1 °C and for warmer climate, it is around 30.6 °C (Fig. 5a). For former case, the PV electrical output increases from 178.9 W (in PV-alone) to 194.8 W, 196.3 W, 197.0 W, 197.4 and 197.4 W (in Finned-PV-PCM) for s_f = 1 m, 1/2 m, 1/3 m, 1/4 m and 1/5 m respectively and

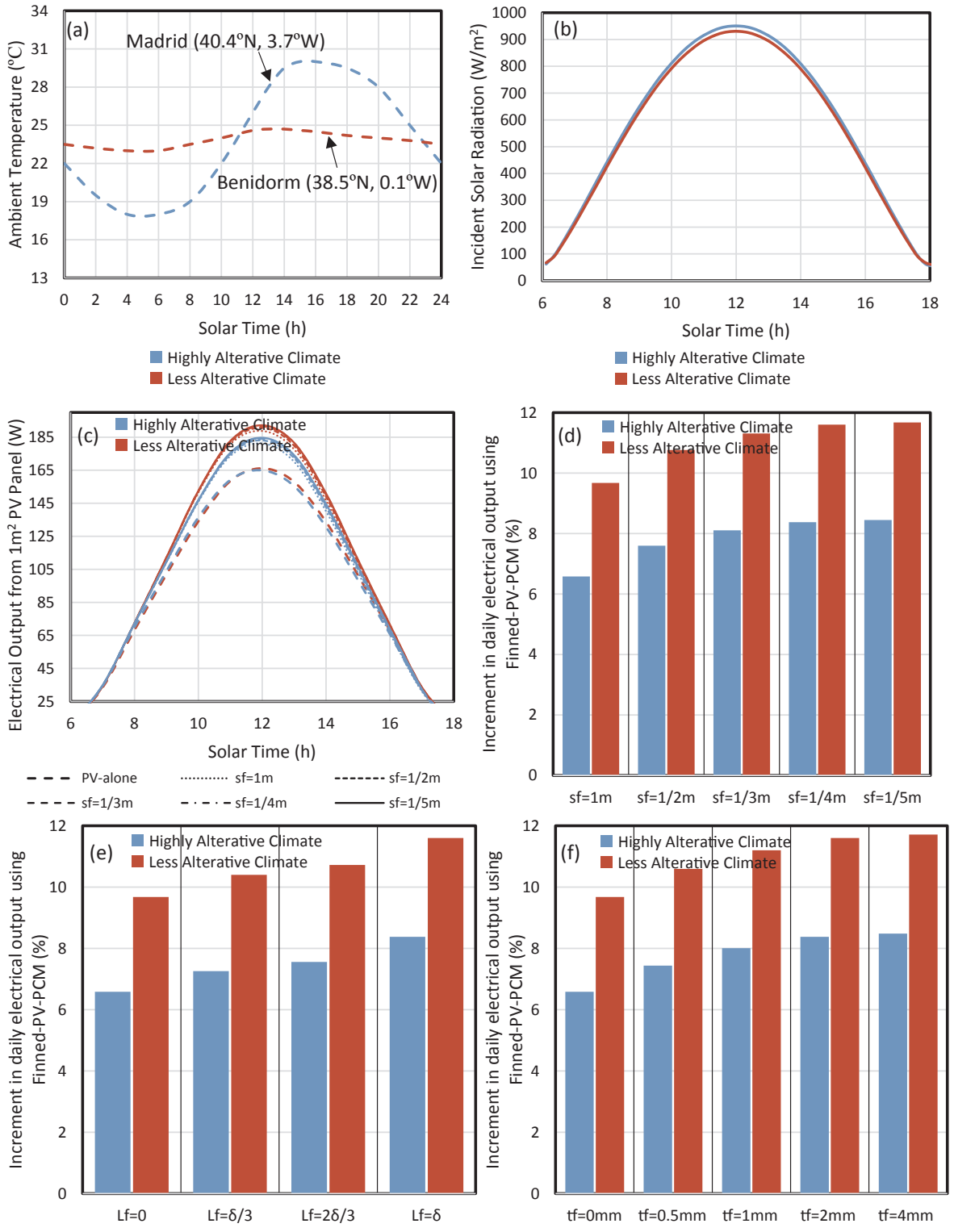

Fig. 4. Electrical output from the PV-alone and Finned-PCM integrated PV systems for various fin geometries for highly alterative and less alterative climates keeping s_f = 25 cm, L_f = δ and t_f = 2 mm wherever fixed.

for latter case, it increases from 157.2 W (in PV-alone) to 181.0 W, 182.9 W, 183.9 W, 184.4 W and 184.4 W (in Finned-PV-PCM) for respective s_f values (Fig. 5c).

The results show that for colder climate, the increments in electrical output using finned phase change material are 5.4%, 6.1%, 6.5%, 6.7% and 6.7% for s_f = 1 m, 1/2 m, 1/3 m, 1/4 m and 1/5 m respectively (Fig. 5d), 5.8%, 6.1% and 6.7% for L_f = δ/3, 2δ/3 and δ respectively (Fig. 5e) and 5.9%, 6.4%, 6.7% and 6.7% for t_f = 0.5 mm, 1 mm, 2 mm and 4 mm respectively (Fig. 5f).

For warmer climate, the enhancements in electrical output using finned phase change material increase to 10.1%, 11.3%, 11.8%, 12.1% and 12.1% for s_f = 1 m, 1/2 m, 1/3 m, 1/4 m and 1/5 m respectively (Fig. 5d), 10.9%, 11.2% and 12.1% for L_f = δ/3, 2δ/3 and δ respectively (Fig. 5e) and 11.1%, 11.7%, 12.1% and 12.1% for t_f = 0.5 mm,

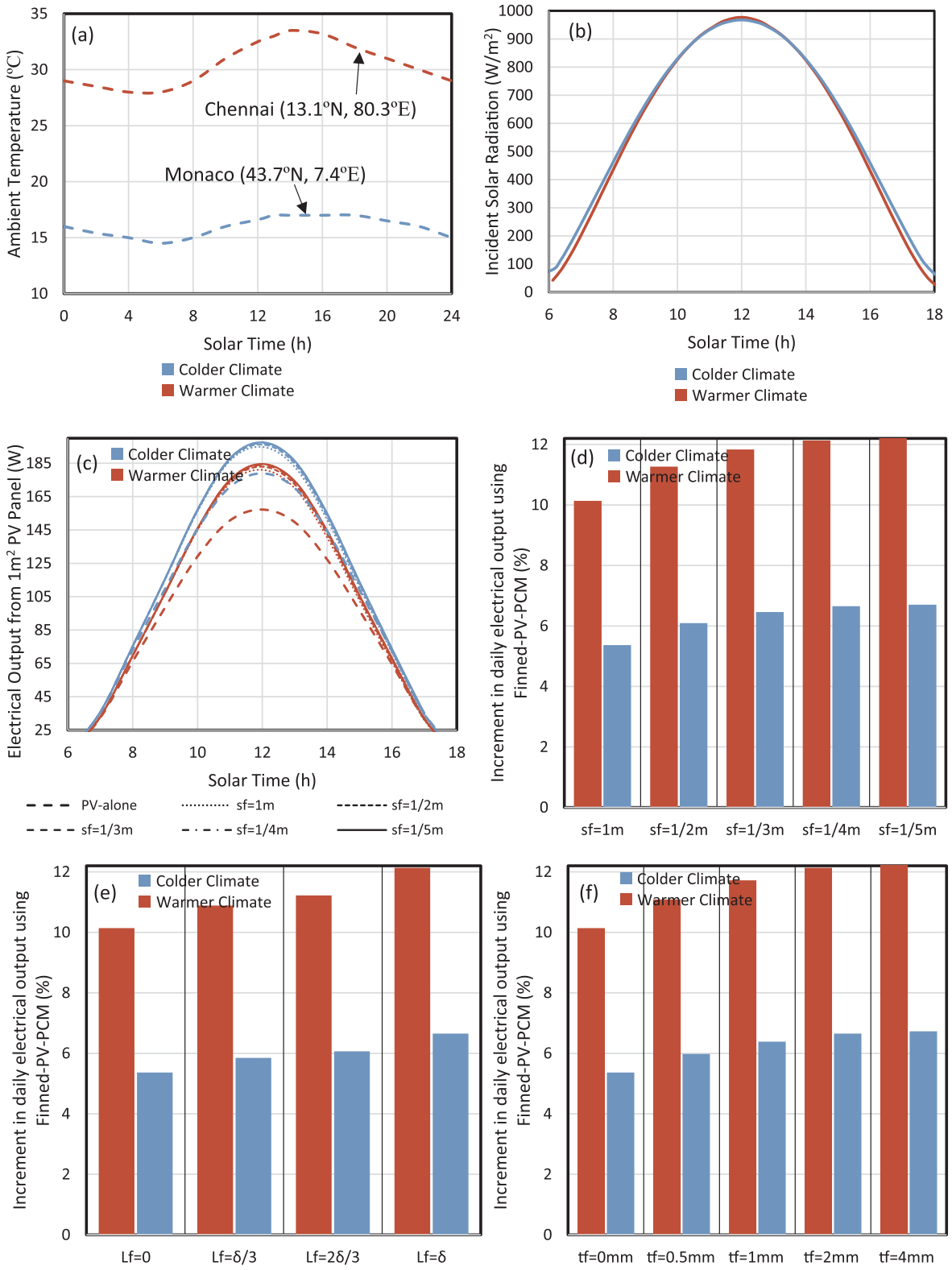

Fig. 5. Electrical output from the PV-alone and Finned-PCM integrated PV systems for various fin geometries for colder and warmer climates keeping s_f = 25 cm, $L_f = \delta$ and t_f = 2 mm wherever fixed.

1 mm, 2 mm and 4 mm respectively (Fig. 5f).

From the results, it can be inferred that if climates are colder, use of finned phase change material is lesser effective idea. Because, colder climates keep cooling the PV systems already leaving less substantial scope for improving performance through finned phase change material.

5.3. Windy vs lesser windy climates

For different fin geometries, the electrical outputs from the two systems are found out for windy and lesser windy climates and have been presented in Fig. 6. For windy climate, the average wind velocity

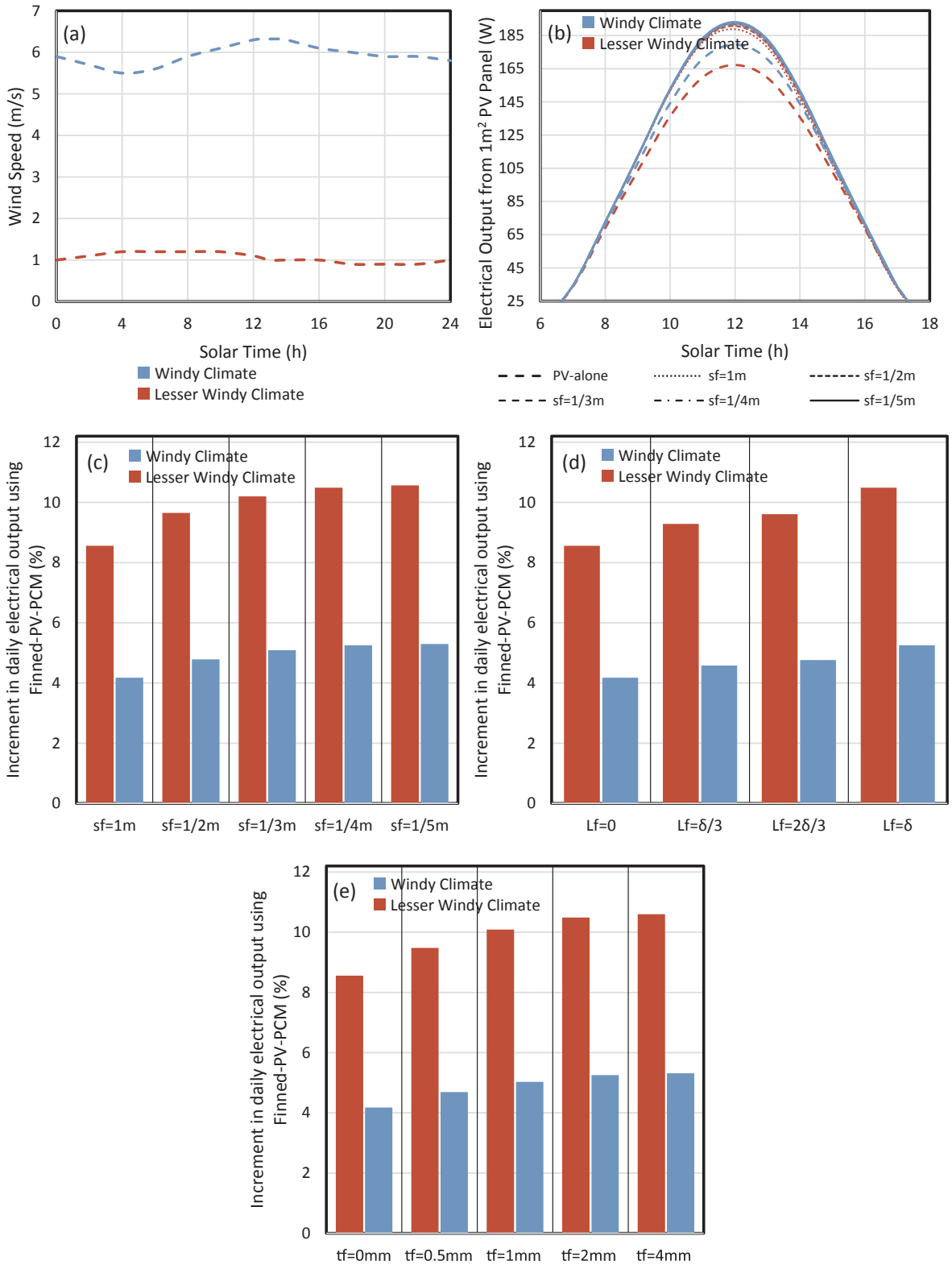

Fig. 6. Electrical output from the PV-alone and Finned-PCM integrated PV systems for various fin geometries for windy and lesser windy climates keeping s_f = 25 cm, $L_f = \delta$ and t_f = 2 mm wherever fixed.

over the day is around 6.3 m/s and for lesser windy climate, it is around 1.2 m/s (Fig. 6a). For former case, the PV electrical output increases from 179.5 W (in PV-alone) to 191.3 W, 192.3 W, 192.8 W, 193.1 W and 193.1 W (in Finned-PV-PCM) for s_f = 1 m, 1/2 m, 1/3 m, 1/4 m and 1/5 m respectively and for latter case, it increases from 167.2 W (in PV-alone) to 188.9 W, 190.7 W, 191.7 W, 192.2 W and 192.2 W (in Finned-PV-PCM) for respective s_f values (Fig. 6b).

The results show that for windy climate, the increments in electrical output using finned phase change material are 4.2%, 4.8%, 5.1%, 5.3% and 5.3% for s_f = 1 m, 1/2 m, 1/3 m, 1/4 m and 1/5 m respectively (Fig. 6c), 4.6%, 4.8% and 5.3% for $L_f = \delta/3$, $2\delta/3$ and δ respectively (Fig. 6d) and 4.6%, 5.0%, 5.3% and 5.3% for t_f = 0.5 mm, 1 mm, 2 mm

and 4 mm respectively (Fig. 6e).

For lesser windy climate, the enhancements in electrical output using finned phase change material increase to 8.6%, 9.6%, 10.2%, 10.5% and 10.5% for s_f = 1 m, 1/2 m, 1/3 m, 1/4 m and 1/5 m respectively (Fig. 6c), 9.3%, 9.6% and 10.5% for L_f = δ/3, 2δ/3 and δ respectively (Fig. 6d) and 9.4%, 10.1%, 10.5% and 10.5% for t_f = 0.5 mm, 1 mm, 2 mm and 4 mm respectively (Fig. 6e).

To summarise, for windy climates, finned phase change material is lesser useful for cooling PV as speedy winds remove heat on their own reducing the relevance of finned phase change material. It is also found that for windy climates, flow is mixed and for lesser windy climates, flow is laminar.

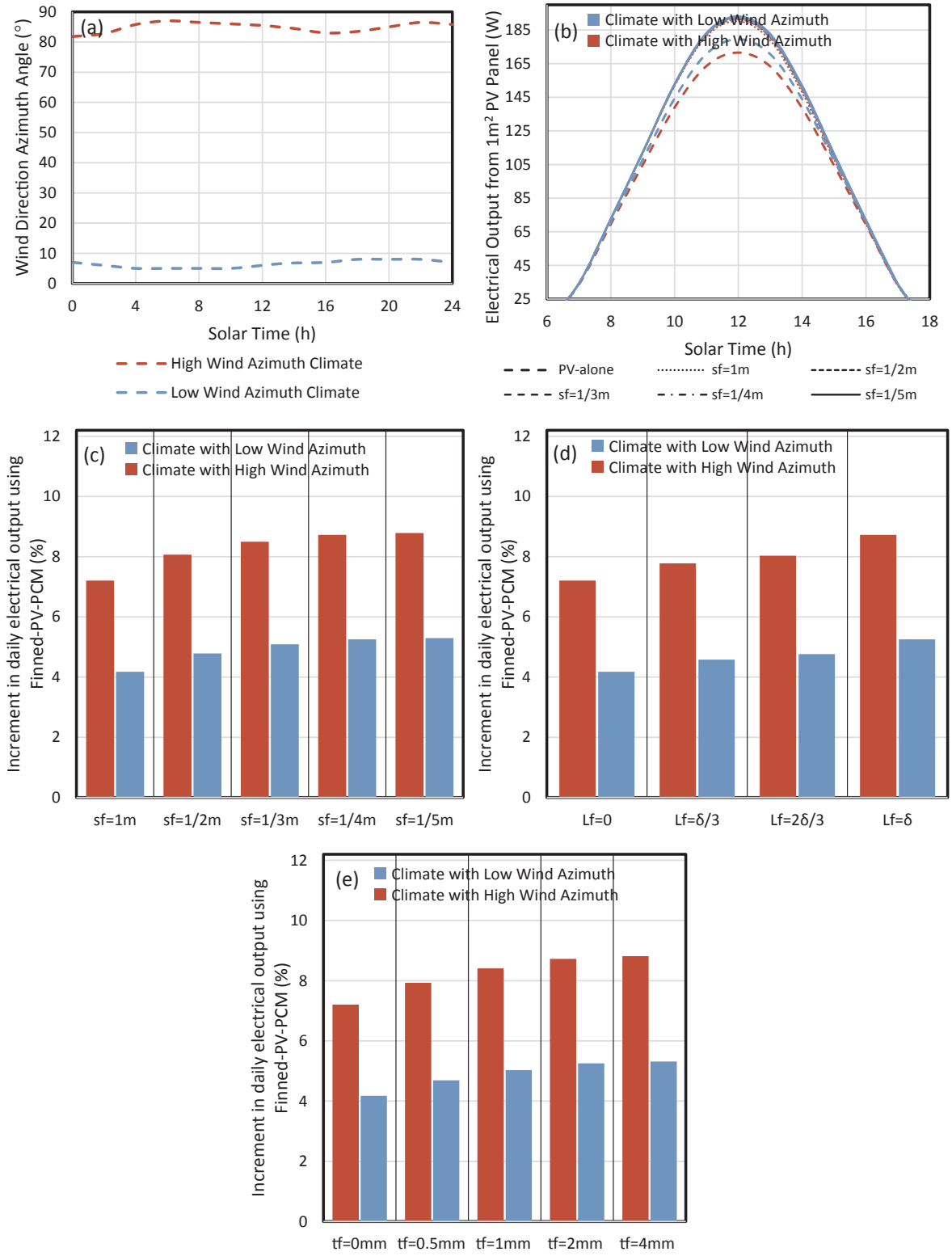

Fig. 7. Electrical output from the PV-alone and Finned-PCM integrated PV systems for various fin geometries for high wind-azimuth and low wind-azimuth climates keeping s_f = 25 cm, L_f = δ and t_f = 2 mm wherever fixed.

5.4. High wind-azimuth vs low wind-azimuth climates

For different fin geometries, the electrical outputs from the two systems are found out for high wind-azimuth and lesser wind-azimuth climates and have been presented in Fig. 7. For high wind-azimuth climate, the average wind-azimuth over the day is around 85° and for low wind-azimuth climate, it is near to 0° (Fig. 7a).

The results show that for high wind-azimuth climate, the increments in electrical output using finned phase change material are 7.2%, 8.1%, 8.5%, 8.7% and 8.7% for s_f = 1 m, 1/2 m, 1/3 m, 1/4 m and 1/5 m respectively (Fig. 7c), 7.8%, 8.1% and 8.7% for L_f = δ/3, 2δ/3 and δ respectively (Fig. 7d) and 7.9%, 8.4%, 8.7% and 8.7% for t_f = 0.5 mm,

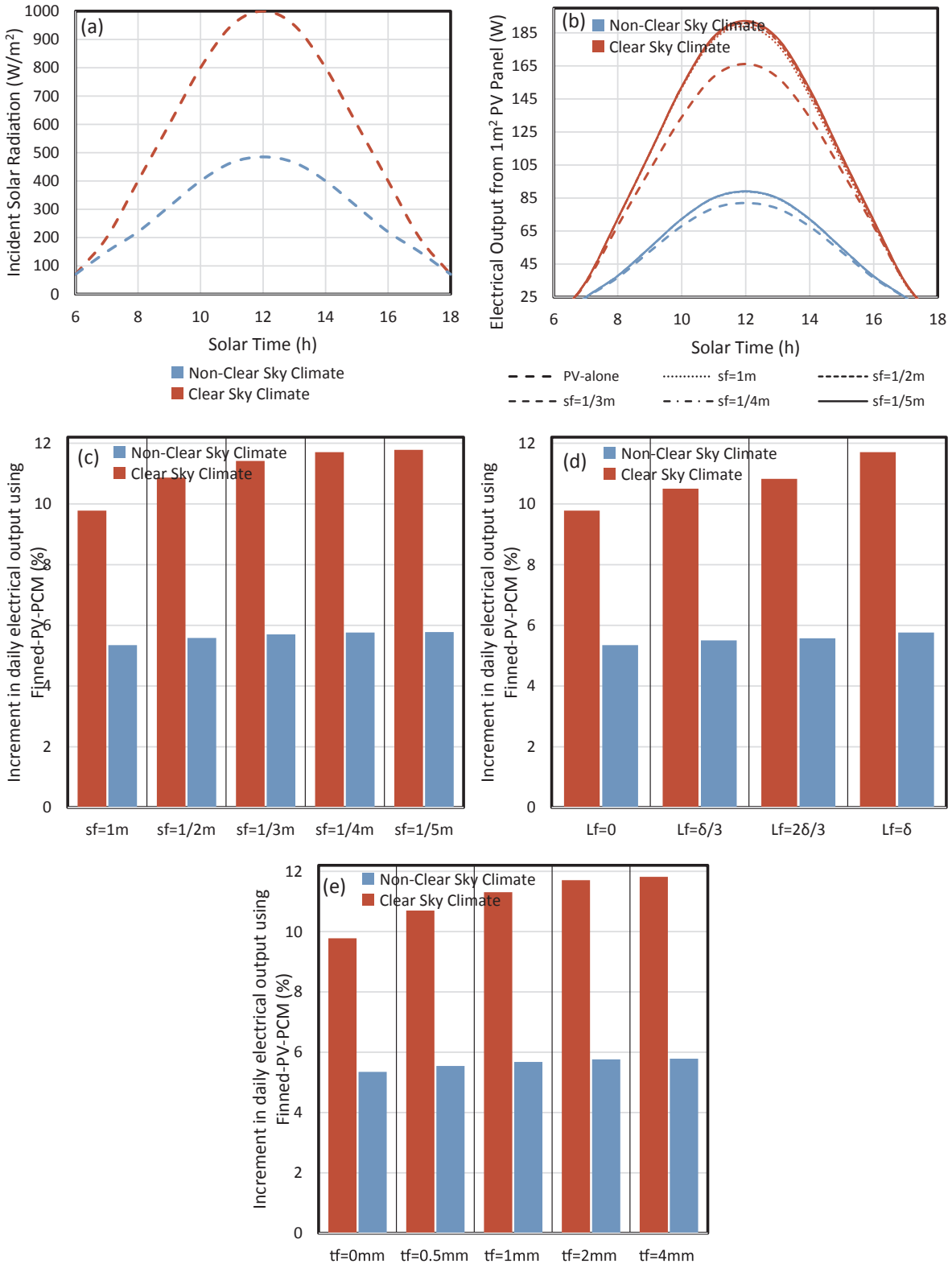

Fig. 8. Electrical output from the PV-alone and Finned-PCM integrated PV systems for various fin geometries for clear sky and non-clear sky climates keeping s_f = 25 cm, L_f = δ and t_f = 2 mm wherever fixed.

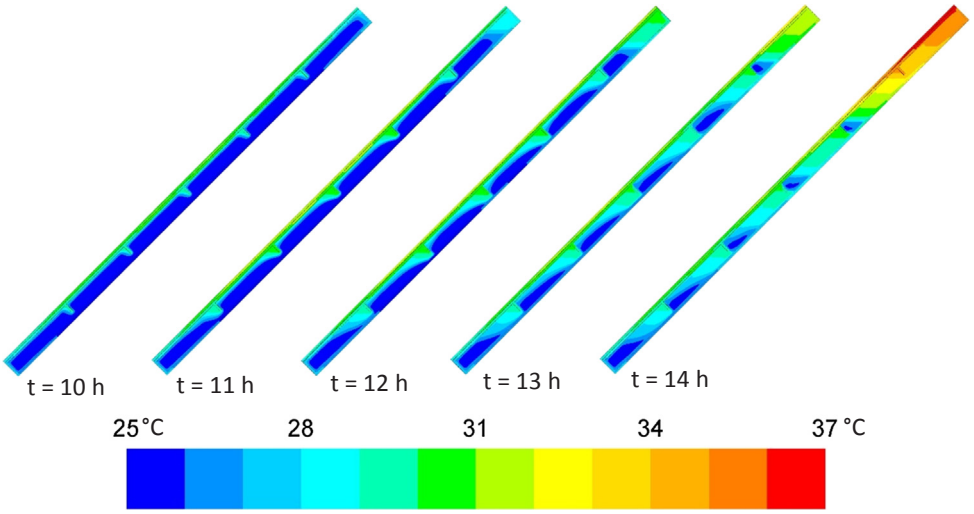

Fig. 9. Variations in the temperature of the system with time.

1 mm, 2 mm and 4 mm respectively (Fig. 7e).

For lesser wind-azimuth climate, the enhancements in electrical output using finned phase change material reduce to 4.2%, 4.8%, 5.1%, 5.3% and 5.3% for s_f = 1 m, 1/2 m, 1/3 m, 1/4 m and 1/5 m respectively (Fig. 7c), 4.6%, 4.8% and 5.3% for $L_f = \delta/3$, $2\delta/3$ and δ respectively (Fig. 7d) and 4.7%, 5.1%, 5.3% and 5.3% for t_f = 0.5 mm, 1 mm, 2 mm and 4 mm respectively (Fig. 7e).

From results, it is evident that climates having winds blowing normally with the PV have lesser relevance for finned phase change material integration. Because, in such cases, the blowing wind itself removes the PV's heat effectively leaving lesser room for additional cooling from finned phase change material.

It is also found that for high wind-azimuth climate, flow is mixed and for low wind-azimuth climate, flow is laminar.

5.5. Clear sky vs non-clear sky climates

For different fin geometries, the electrical outputs from the two systems are found out for clear sky and non-clear sky climates and have been presented in Fig. 8. For clear sky climate, the maximum solar irradiance at PV over the day is around 995 W/m^2 and for non-clear sky, it is near to 490 W/m^2 (Fig. 8a).

The results show that for clear sky climate, the increments in electrical output using finned phase change material are 9.8%, 10.9%, 11.4%, 11.7% and 11.7% for s_f = 1 m, 1/2 m, 1/3 m, 1/4 m and 1/5 m respectively (Fig. 8c), 10.5%, 10.8% and 11.7% for $L_f = \delta/3$, $2\delta/3$ and δ respectively (Fig. 8d) and 10.7%, 11.3%, 11.7% and 11.7% for t_f = 0.5 mm, 1 mm, 2 mm and 4 mm respectively (Fig. 8e).

For non-clear sky climate, the enhancements in electrical output using finned phase change material reduce to 5.3%, 5.6%, 5.7%, 5.8% and 5.8% for s_f = 1 m, 1/2 m, 1/3 m, 1/4 m and 1/5 m respectively (Fig. 8c), 5.5%, 5.6% and 5.8% for $L_f = \delta/3$, $2\delta/3$ and δ respectively (Fig. 8d) and 5.5%, 5.7%, 5.8% and 5.8% for t_f = 0.5 mm, 1 mm, 2 mm and 4 mm respectively (Fig. 8e).

It must be observed that the use of finned phase change material is more beneficial in places having clear sky. The larger solar flux incident in such places produces more heat and thus requires external cooling.

It must be mentioned that during the melting of the PCM, the thermal variations inside the PCM container leads to non-uniform PV temperature as shown in Fig. 9. Thus, average PV temperature is used to calculate the electrical output for all the above results.

6. Conclusions

Current investigation involves the modelling of system which has been validated using experimental results. It also involves the computation of power produced and its dependency on time and different climates. Fins with different spacings (s_f), thicknesses (t_f) and lengths (L_f) have been studied. The improvement in power production with effective cooling in case of Finned-PV-PCM is reported too. The main conclusions of the study are

(i) For highly alterative climate, the increments in electrical output using finned phase change material are 6.6%, 7.6%, 8.1%, 8.4% and 8.4% for s_f = 1 m, 1/2 m, 1/3 m, 1/4 m and 1/5 m respectively, 7.3%, 7.6% and 8.4% for $L_f = \delta/3$, $2\delta/3$ and δ respectively and 7.4%, 8.0%, 8.4% and 8.4% for t_f = 0.5 mm, 1 mm, 2 mm and 4 mm respectively. For less alterative climate, the enhancements in electrical output increase to 9.7%, 10.8%, 11.3%, 11.6% and 11.6% for different spacings, 10.4%, 10.7% and 11.6% for different lengths and 10.6%, 11.2%, 11.6% and 11.6% respectively for different thicknesses.
(ii) To increase the power output from finned PCM integrated PV, the most suitable fin geometry has been found as 25 cm of fins' spacing, length as box's depth and thickness as 2 mm.
(iii) For warmer climate, the increments in electrical output using finned phase change material reach to 12.1% and for colder climate, the increment is only 6.7%.
(iv) For windy climate, the increment in electrical output using finned PCM is 5.3% and for lesser windy climate, the increment is 10.5%.
(v) For high wind azimuth climate, the increments in electrical output using finned PCM are larger than that of low wind azimuth climate.
(vi) Finned phase change material is more beneficial for climate having clear sky. The larger solar flux incident in such places produces more heat and thus requires external cooling.

Acknowledgement

The authors gratefully acknowledge the financial support from Engineering and Physical Sciences Research Council funded Reliable and Efficient System for Community Energy Solution - RESCUES project (Grant Number: EP/K03619X/1). In support of open access research, all underlying article materials (such as data, samples or models) can be accessed upon request via email to the corresponding author.

References

Al Siyabi, I., Khanna, S., Mallick, T., Sundaram, S., 2018. Electricity enhancement and thermal energy production from concentrated photovoltaic integrated with a 3-

layered stacked micro-channel heat sink. In: AIP Conference Proceedings 2012, 080001. doi: 10.1063/1.5053529.
Al Siyabi, I., Khanna, S., Mallick, T., Sundaram, S., 2018b. Multiple Phase Change Material (PCM) configuration for PCM-based heat sinks—an experimental study. Energies 11 (7), 1629.
Atkin, P., Farid, M.M., 2015. Improving the efficiency of photovoltaic cells using PCM infused graphite and aluminium fins. Sol. Energy 114, 217–228.
Baygi, S.R.M., Sadrameli, S.M., 2018. Thermal management of photovoltaic solar cells using polyethylene glycol 1000 (PEG1000) as a phase change material. Therm. Sci. Eng. Progr. 5, 405–411.
Biwole, P.H., Eclache, P., Kuznik, F., 2013. Phase-change materials to improve solar panel's performance. Energy Build. 62, 59–67.
Biwole, P.H., Groulx, D., Souayfane, F., Chiu, T., 2018. Influence of fin size and distribution on solid-liquid phase change in a rectangular enclosure. Int. J. Therm. Sci. 124, 433–446.
Brano, V.L., Ciulla, G., Piacentino, A., Cardona, F., 2014. Finite difference thermal model of a latent heat storage system coupled with a photovoltaic device: description and experimental validation. Renew. Energy 68, 181–193.
Browne, M.C., Lawlor, K., Kelly, A., Norton, B., McCormack, S.J., 2015. Indoor characterisation of a photovoltaic/thermal phase change material system. Energy Procedia 70, 163–171.
Browne, M.C., Norton, B., McCormack, S.J., 2015. Phase change materials for photovoltaic thermal management. Renew. Sustain. Energy Rev. 47, 762–782.
Browne, M.C., Norton, B., McCormack, S.J., 2016a. Heat retention of a photovoltaic/thermal collector with PCM. Sol. Energy 133, 533–548.
Browne, M.C., Quigley, D., Hard, H.R., Gilligan, S., Ribeiro, N.C.C., Almeida, N., McCormack, S.J., 2016b. Assessing the thermal performance of phase change material in a photovoltaic/thermal system. Energy Procedia 91, 113–121.
Chandel, S.S., Agarwal, T., 2017. Review of cooling techniques using phase change materials for enhancing efficiency of photovoltaic power systems. Renew. Sustain. Energy Rev. 73, 1342–1351.
Ciulla, G., Brano, V.L., Cellura, M., Franzitta, V., Milone, D., 2012. A finite difference model of a PV-PCM system. Energy Procedia 30, 198–206.
Cui, T., Xuan, Y., Li, Q., 2016. Design of a novel concentrating photovoltaic–thermoelectric system incorporated with phase change materials. Energy Convers. Manage. 112, 49–60.
Du, D., Darkwa, J., Kokogiannakis, G., 2013. Thermal management systems for Photovoltaics (PV) installations: a critical review. Sol. Energy 97, 238–254.
Emam, M., Ahmed, A., 2018. Cooling concentrator photovoltaic systems using various configurations of phase-change material heat sinks. Energy Convers. Manage. 158, 298–314.
Emam, M., Ookawara, S., Ahmed, M., 2017. Performance study and analysis of an inclined concentrated photovoltaic-phase change material system. Sol. Energy 150, 229–245.
Groulx D., Biwole P.H., 2014. Solar PV passive temperature control using phase change materials. In: 15th International Heat Transfer Conference, August 10–15, 2014, Kyoto, Japan.
Hasan, A., McCormack, S.J., Huang, M.J., Norton, B., 2010. Evaluation of phase change materials for thermal regulation enhancement of building integrated photovoltaics. Sol. Energy 84, 1601–1612.
Hasan, A., McCormack, S.J., Huang, M.J., Sarwar, J., Norton, B., 2015. Increased photovoltaic performance through temperature regulation by phase change materials: Materials comparison in different climates. Sol. Energy 115, 264–276.
Huang, M.J., Eames, P.C., Norton, B., 2004. Thermal regulation of building-integrated photovoltaics using phase change materials. Int. J. Heat Mass Transf. 47, 2715–2733.
Huang, M.J., Eames, P.C., Norton, B., 2006. Phase change materials for limiting temperature rise in building integrated photovoltaics. Sol. Energy 80, 1121–1130.
Huang, M.J., Eames, P.C., Norton, B., 2007. Comparison of predictions made using a new 3D phase change material thermal control model with experimental measurements and predictions made using a validated 2D model. Heat Transfer Eng. 28, 31–37.
Huang, M.J., Eames, P.C., Norton, B., Hewitt, N.J., 2011. Natural convection in an internally finned phase change material heat sink for the thermal management of photovoltaics. Sol. Energy Mater. Sol. Cells 95, 1598–1603.
Indartono, Y.S., Suwono, A., Pratama, F.Y., 2014. Improving photovoltaics performance by using yellow petroleum jelly as phase change material. Int. J. Low-Carbon Technol. 1–5.
Kamkari, B., Groulx, D., 2018. Experimental investigation of melting behaviour of phase change material in finned rectangular enclosures under different inclination angles. Exp. Therm Fluid Sci. 97, 94–108.
Kant, K., Shukla, A., Sharma, A., Biwole, P.H., 2016. Heat transfer studies of photovoltaic panel coupled with phase change material. Sol. Energy 140, 151–161.
Kaplani, E., Kaplanis, S., 2014. Thermal modelling and experimental assessment of the dependence of PV module temperature on wind velocity and direction, module orientation and inclination. Sol. Energy 107, 443–460.
Khanna, S., Reddy, K.S., Mallick, T.K., 2018. Photovoltaic system integrated with phase change material for South West UK climate. In: AIP Conference Proceedings 2012, 080007. doi: 10.1063/1.5053535.
Khanna, S., Sharma, V., 2015. Effect of number of supports on the bending of absorber tube of parabolic trough concentrator. Energy 93, 1788–1803.
Khanna, S., Sharma, V., 2016. Explicit analytical expression for solar flux distribution on an undeflected absorber tube of parabolic trough concentrator considering sun-shape and optical errors. J. Sol. Energy Eng. 138, 011010–11110.
Khanna, S., Singh, S., Kedare, S.B., 2014. Effect of angle of incidence of sun rays on the bending of absorber tube of solar parabolic trough concentrator. Energy Procedia 48, 123–129.
Khanna, S., Sharma, V., Kedare, S.B., Singh, S., 2016. Experimental investigation of the bending of absorber tube of solar parabolic trough concentrator and comparison with analytical results. Sol. Energy 125, 1–11.
Khanna, S., Sharma, V., Singh, S., Kedare, S.B., 2016. Explicit expression for temperature distribution of receiver of parabolic trough concentrator considering bimetallic absorber tube. Appl. Therm. Eng. 103, 323–332.
Khanna, S., Reddy, K.S., Mallick, T.K., 2017. Performance analysis of tilted photovoltaic system integrated with phase change material under varying operating conditions. Energy 133, 887–899.
Khanna, S., Sundaram, S., Reddy, K.S., Mallick, T.K., 2017. Performance analysis of perovskite and dye-sensitized solar cells under varying operating conditions and comparison with monocrystalline silicon cell. Appl. Therm. Eng. 127, 559–565.
Khanna, S., Reddy, K.S., Mallick, T.K., 2018e. Climatic behaviour of solar photovoltaic integrated with phase change material. Energy Convers. Manage. 166, 590–601.
Khanna, S., Reddy, K.S., Mallick, T.K., 2018a. Optimization of solar photovoltaic system integrated with phase change material. Sol. Energy 163, 591–599.
Khanna, S., Reddy, K.S., Mallick, T.K., 2018c. Optimization of fins fitted phase change material equipped photovoltaic under various working circumstances. Energy Convers. Manage.
Khanna, S., Reddy, K.S., Mallick, T.K., 2018b. Optimization of finned solar photovoltaic phase change material (Finned PV PCM) system. Int. J. Therm. Sci. 130, 313–322.
Khanna, S., Reddy, K.S., Mallick, T.K., 2018. Electrical enhancement of solar photovoltaic using fins enabled phase change material exposed to diverse working circumstances, J. Cleaner Prod. (yet to be published).
Kibria, M.A., Saidur, R., Al-Sulaiman, F.A., Aziz, M.M.A., 2016. Development of a thermal model for a hybrid photovoltaic module and phase change materials storage integrated in buildings. Sol. Energy 124, 114–123.
Ma, T., Yang, H., Zhang, Y., Lu, L., Wang, X., 2015. Using phase change materials in photovoltaic systems for thermal regulation and electrical efficiency improvement: a review and outlook. Renew. Sustain. Energy Rev. 43, 1273–1284.
Mahamudul, H., Rahman, M.M., Metselaar, H.S.C., Mekhilef, S., Shezan, S.A., Sohel, R., Karim, S.B.A., Badiuzaman, W.N.I., 2016. Temperature regulation of photovoltaic module using phase change material: a numerical analysis and experimental investigation. Int. J. Photoenergy 5917028, 1–8.
Park, J., Kim, T., Leigh, S.B., 2014. Application of a phase-change material to improve the electrical performance of vertical-building-added photovoltaics considering the annual weather conditions. Sol. Energy 105, 561–674.
Preet, S., 2018. Water and phase change material based photovoltaic thermal management systems: a review. Renew. Sustain. Energy Rev. 82, 791–807.
Preet, S., Bhushan, B., Mahajan, T., 2017. Experimental investigation of water based photovoltaic/thermal (PV/T) system with and without phase change material (PCM). Sol. Energy 155, 1104–1120.
Rubitherm Phase Change Material < https://www.rubitherm.eu/ > (accessed 08.01. 2018).
Sharma, V., Khanna, S., Nayak, J.K., Kedare, S.B., 2016. Effects of shading and blocking in compact linear Fresnel reflector field. Energy 94, 633–653.
Sharma, S., Tahir, A., Reddy, K.S., Mallick, T.K., 2016. Performance enhancement of a building-integrated concentrating photovoltaic system using phase change material. Sol. Energy Mater. Sol. Cells 149, 29–39.
Sharma, S., Micheli, L., Chang, W., Tahir, A., Reddy, K.S., Mallick, T.K., 2017. Nano-enhanced Phase Change Material for thermal management of BICPV. Appl. Energy 208, 719–733.
Shukla, A., Kant, K., Sharma, A., Biwole, P.H., 2017. Cooling methodologies of photovoltaic module for enhancing electrical efficiency: a review. Sol. Energy Mater. Sol. Cells 160, 275–286.
Su, D., Jia, Y., Alva, G., Liu, L., Fang, G., 2017a. Comparative analyses on dynamic performances of photovoltaic–thermal solar collectors integrated with phase change materials. Energy Convers. Manage. 131, 79–89.
Su, D., Jia, Y., Lin, Y., Fang, G., 2017b. Maximizing the energy output of a photovoltaic–thermal solar collector incorporating phase change materials. Energy Build. 153, 382–391.
Su, Y., Zhang, Y., Shu, L., 2018. Experimental study of using phase change material cooling in a solar tracking concentrated photovoltaic-thermal system. Sol. Energy 159, 777–785.